Umklapp scattering in the one-dimensional Hubbard model

Tong Liu,[1,2] Kang Wang,[1,2] Runze Chi,[1,2] Yang Liu,[1,2] Haijun Liao,[1,3,*] and T. Xiang[1,4,2,†]

[1]*Institute of Physics, Chinese Academy of Sciences, Beijing 100190, China*
[2]*School of Physical Sciences, University of Chinese Academy of Sciences, Beijing 100049, China*
[3]*Songshan Lake Materials Laboratory, Dongguan, Guangdong 523808, China*
[4]*Beijing Academy of Quantum Information Sciences, Beijing 100190, China*

(Received 17 February 2023; revised 1 September 2023; accepted 5 September 2023; published 21 September 2023)

The one-dimensional Mott metal-insulator transition is a typical strong correlation effect triggered by the Umklapp scattering. However, in a physical system, the Umklapp scattering coexists with the normal scattering, including both forward and backward scattering, which conserves the total momentum of scattered electrons. Therefore, it is not easy to quantify the contribution of the Umklapp scattering in a Mott metal-insulator transition. To resolve this difficulty, we propose to explore these scattering processes separately. We study the contribution of each scattering process in the one-dimensional Hubbard model using the momentum-space density-matrix renormalization group (kDMRG) and bosonization methods. Our kDMRG calculation confirms that the Mott charge gap results from the Umklapp scattering, but the normal scattering processes strongly renormalize its value. Furthermore, we present a scaling analysis of the Mott charge gap in the bosonization theory and show that the interplay between the Umklapp and forward scattering dictates the charge dynamics in the half-filled Hubbard model.

DOI: 10.1103/PhysRevB.108.125134

I. INTRODUCTION

The Mott insulator has gained intensive attention from condensed matter physicists [1–8], not only because the Mott insulator serves as a platform for studying strong correlation effects, but also by doping Mott insulator, we can get many novel phases, such as high-T_c superconductor, pseudogap, non-Fermi liquid, charge density wave, etc. [9–14]. This interaction-driven effect could be understood qualitatively using the Hubbard model at half-filling [15,16]. The Hubbard system is metallic in the weak-coupling limit, where the on-site Coulomb interaction is small compared to the kinetic energy. However, in the strong-coupling limit, the on-site Hubbard interaction dictates the conducting behaviors. It tends to localize electrons by raising the energy of double occupation on a single lattice site, which opens a charge excitation gap at half-filling. Therefore, the half-filled Hubbard system undergoes a Mott metal-insulator transition from the weak to strong coupling limit.

The Hubbard interaction can be decomposed into three terms according to their scattering processes: forward, backward, and Umklapp scattering. Both the forward and backward scattering processes conserve the total momentum of electrons. They correlate electrons in the ferromagnetic and antiferromagnetic channels, respectively. However, the Umklapp process conserves the total momentum of scattered electrons up to a reciprocal-lattice vector. This process is greatly enhanced around the half-filling and is the driving force that is responsible for the formation of the Mott insulating gap. In the band theory, a half-filled band is a metal rather than an insulator. However, the Umklapp scattering bounces two electrons in the vicinity of one side of the Fermi surface to the opposite side in one dimension, leading to a charge excitation gap with divergent charge compressibility at half-filling [17–20]. The Umklapp process might be responsible for the pseudogap phenomenon observed in high-T_c copper oxides [21,22]. It can also induce a topologically nontrivial edge state [23].

A thorough investigation of the Umklapp scattering is essential to a qualitative understanding of the Mott physics [24–29]. However, it is difficult to investigate the Umklapp process because it coexists with the forward and backward processes in real materials. Their interplay makes it hard to unveil the secret of the Umklapp scattering. Nevertheless, in theoretical studies, we can separate these scattering processes and consider the contribution of each process independently, allowing us to quantitatively investigate the effect of the Umklapp scattering on the Mott insulating transition and how it interferes with other processes.

In this work, we present a comparative study of the Hubbard model and a modified Hubbard model, which contains only the Umklapp scattering term, namely ignoring the forward and backward scattering terms, in the on-site Coulomb interactions. We call this modified Hubbard model the Umklapp model. The one-dimensional Hubbard model is soluble by the Bethe ansatz [30,31]. It can also be accurately probed by the real-space density-matrix renormalization group (DMRG) [32,33] and quantum Monte Carlo [34]. However, it is much more challenging to solve the Umklapp model. First, the Bethe ansatz does not work for this

*navyphysics@iphy.ac.cn
†txiang@iphy.ac.cn

model. Furthermore, there are technical barriers in carrying out real-space DMRG and quantum Monte Carlo simulations for this model because the Umklapp scattering potential is long-ranged and suffers from the minus-sign problem even at half-filling.

We propose to use the momentum-space DMRG (kDMRG) [35], combined with a scaling analysis of the coupling constants in the framework of bosonization [36], to resolve the above difficulties. kDMRG is an effective method for exploring this problem because the Umklapp scattering potential takes a relatively simple representation in momentum space. The scaling analysis, on the other hand, allows us to gain a clearer picture of how the interplay between different scattering processes affects the Mott insulating behavior [17,37].

II. MODEL

The one-dimensional Hubbard model is described by the Hamiltonian:

$$H = -t\sum_{j\sigma}(c^{\dagger}_{j\sigma}c_{j+1,\sigma} + \text{H.c.}) + U\sum_{j} n_{j\uparrow}n_{j\downarrow}, \qquad (1)$$

where $c_{j\sigma}$ is the annihilation operator of an electron at site j with spin σ, and $n_{j\sigma} = c^{\dagger}_{j\sigma}c_{j\sigma}$. In momentum space, it becomes

$$H = -2t\sum_{k\sigma}\cos k c^{\dagger}_{k\sigma}c_{k\sigma} + H_n + H_u \qquad (2)$$

$$H_n = \frac{U_1}{L}\sum_{k_1k_2k_3k_4} c^{\dagger}_{k_1\uparrow}c_{k_2\uparrow}c^{\dagger}_{k_3\downarrow}c_{k_4\downarrow}\delta_{k_1+k_3,k_2+k_4}, \qquad (3)$$

$$H_u = \frac{U_2}{L}\sum_{k_1k_2k_3k_4} c^{\dagger}_{k_1\uparrow}c_{k_2\uparrow}c^{\dagger}_{k_3\downarrow}c_{k_4\downarrow}\delta_{k_1+k_3,k_2+k_4\pm 2\pi}, \qquad (4)$$

where L is the system size. Here we separate the Coulomb interaction terms into two parts according to the scattering processes. H_n is the Hamiltonian of normal scattering, including both forward and backward scattering, which preserves the total momentum. H_u, on the other hand, is the Hamiltonian of the Umklapp scattering, which preserves the total momentum up to a reciprocal lattice vector. To distinguish these terms explicitly, we assume H_n and H_u to have different coupling constants, U_1 and U_2.

The Hubbard model (1) corresponds to the case $U_1 = U_2 = U$. We can screen the normal scattering process by setting $U_1 = 0$. In that case, H is just the Hamiltonian of the Umklapp model. Similarly, we can switch off the Umklapp scattering by setting $U_2 = 0$ and refer to the resulting Hamiltonian as the non-Umklapp model. The Hubbard interaction is local in real space. However, for the above generalized Hubbard model, the interaction becomes highly nonlocal when transformed back from the momentum-space representation to real space in the case $U_1 \neq U_2$.

III. RESULTS OF kDMRG

The traditional implementation of kDMRG involves labeling each local site by momentum, resulting in a four-dimensional Hilbert space at each lattice site. To enhance computational efficiency and obtain spin-resolved mutual information, we modify this approach by dividing a single momentum point into two momentum-spin points with the same momentum but opposite spin. A crucial step in the kDMRG calculation is determining an optimized path to order these momentum-spin points in a one-dimensional chain. As detailed in the Appendix, we achieve this optimization by minimizing the mutual-information distance of all such points. To ensure numerical stability and avoid issues arising from kinetic energy degeneracy, we limit our calculations to systems with a size of $L = 4n + 2$ (where n is an integer) and adopt periodic boundary conditions. The kDMRG results presented in the subsequent discussion are obtained by retaining up to 8000 states, and the tolerance for convergence is set such that the error of the ground-state energy is less than 10^{-6}. A kDMRG calculation for the ground state of a $L = 30$ system by keeping 8000 can be finished in one day using a medium-size workstation.

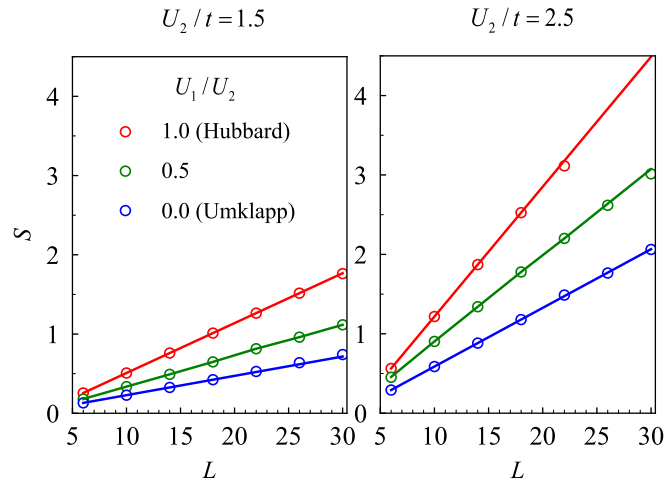

FIG. 1. Comparison of the size dependence of the maximal entanglement entropy S calculated by kDMRG for the ground states of the generalized Hubbard models with $U_1/U_2 = 1$ (Hubbard), $U_1/U_2 = 0.5$, and $U_1/U_2 = 0.0$ (Umklapp).

In momentum space, it is known that the entanglement entropy S of the ground state scales linearly with the system size L for the Hubbard model [38]. Hence the ground state of the Hubbard model satisfies an entanglement volume law in momentum space. Our kDMRG calculation confirms this volume-law behavior of the entanglement entropy for the Hubbard model.

Figure 1 shows the entanglement entropy S of the ground state obtained from the kDMRG calculations for the Umklapp and Hubbard models. For the Umklapp model, the entanglement entropy S also scales linearly with the system size. However, the entanglement entropy of the Umklapp model is much lower than that of the Hubbard model. For the two cases shown in Fig. 1, the entanglement entropy of the Umklapp model is about half of the Hubbard model. It implies that one can reliably study much larger lattice systems for the Umklapp model than for the Hubbard model using kDMRG by keeping the same number of basis states.

The key parameter characterizing a Mott insulating phase is the charge excitation gap, Δ_c, defined by the energy increase in adding and removing a pair of spin-singlet electrons

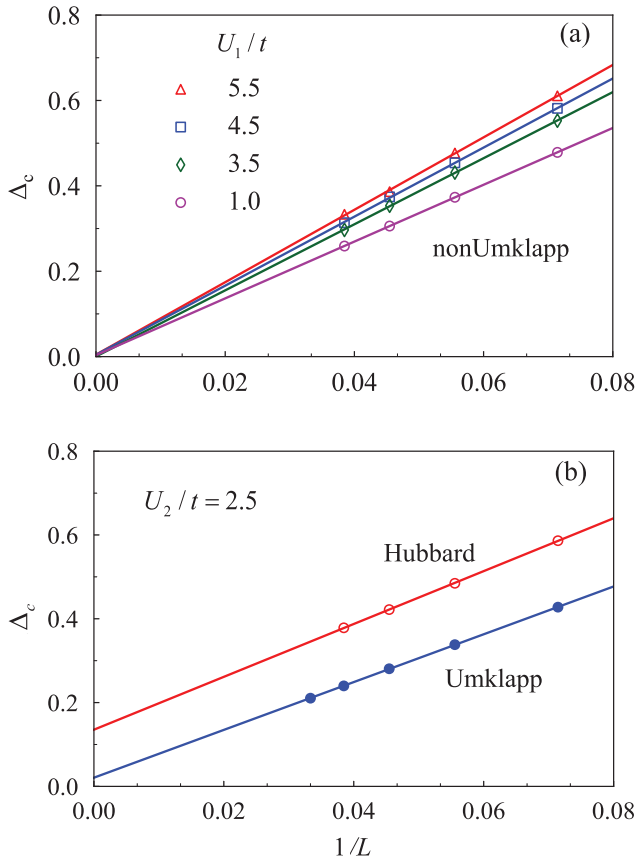

FIG. 2. Charge excitation gap Δ_c as a function of $1/L$ for (a) the non-Umklapp model ($U_2 = 0$) and (b) the Hubbard ($U_1 = U_2$) and Umklapp ($U_1 = 0$) models obtained with kDMRG. The lines are linear fits to the kDMRG data. The extrapolated charge gap of the Hubbard model is 0.135 ± 0.002. The corresponding charge gap of the Umklapp model is 0.021 ± 0.001.

from the half-filled system:

$$\Delta_c(L) = \tfrac{1}{4}[E_g(L+2) + E_g(L-2) - 2E_g(L)], \quad (5)$$

where L is the lattice size and $E_g(N_e)$ is the ground state energy of the system with the electron number N_e. N_e equals L at half-filling.

Figure 2(a) shows the kDMRG result of Δ_c as a function of the inverse lattice length $1/L$ in the absence of the Umklapp scattering ($U_2 = 0$). In this case, Δ_c scales linearly with $1/L$ within numerical errors. By linear extrapolation, we find that the excitation gap vanishes in the thermodynamic limit. Thus the system remains gapless no matter how strong the normal scattering interaction U_1 is.

However, in the presence of the Umklapp scattering, the charge excitation spectrum is gapped. Figure 2(b) compared the size dependence of the charge gap Δ_c for the Hubbard and Umklapp models at half-filling. Again, Δ_c scales linearly with $1/L$ within numerical errors, but the extrapolated gap value in the thermodynamic limit $L \to \infty$ is finite. Moreover, the Umklapp scattering also changes the momentum distribution of electrons when two more electrons are added to the half-filled system. As shown in Fig. 6 in Appendix, the momentum distribution function is mirror symmetric about the $k = 0$ point in the Hubbard model, and the total momentum of the ground state is zero. For the Umklapp model, however, the two added electrons tend to have the same momentum, which breaks the mirror symmetry in the momentum distribution function

The above discussion confirms that the Mott insulating gap arises from the Umklapp scattering rather than the normal scattering processes. However, by comparing the gap value of the Umklapp model with those of the Hubbard model ($U_1/U_2 = 1$) and the model with $U_1/U_2 = 0.5$, we find that the normal scattering processes can significantly enhance the value of the Mott gap once it is open.

IV. SCALING ANALYSIS

To understand the physics underlying the enhancement of the Mott charge gap by the normal scattering, we perform a scaling analysis for the generalized Hubbard model in the bosonization theory. In the long-wavelength limit, the charge and spin excitation spectra in the Hubbard model are separated and effectively described by two boson fields. Following the standard bosonization scheme, it is straightforward to show that the following two Hamiltonians govern the charge and spin dynamical properties of the Hubbard model:

$$H_c = \frac{v_F a}{2}\int dx\left[\Pi_c^2 + \left(1 + \frac{U_1}{\pi v_F}\right)(\partial_x\phi_c)^2 + \frac{U_2\cos\sqrt{8\pi}\phi_c}{v_F\pi^2\alpha^2}\right], \quad (6)$$

$$H_s = \frac{v_F a}{2}\int dx\left[\Pi_s^2 + \left(1 - \frac{U_1}{\pi v_F}\right)(\partial_x\phi_s)^2 + \frac{U_2\cos\sqrt{8\pi}\phi_s}{v_F\pi^2\alpha^2}\right], \quad (7)$$

where ϕ_c and ϕ_s are the boson fields in the charge and spin channels, respectively. Π_σ ($\sigma = c, s$) is the conjugate field of ϕ_σ. α is the inverse of the momentum cutoff. a is lattice constant. To compare with numerical results, a should be set as 1.

In H_c, the U_1 term results from the forward scattering terms in H_n. However, the U_1 term in H_s is the contribution of the backward scattering. Thus the backward scattering affects the spin dynamics but not the charge dynamics. These U_1 terms renormalize the charge and spin velocities to

$$v_c = v_F\left(1 + \frac{U_1 a}{2\pi v_F}\right), \quad v_s = v_F\left(1 - \frac{U_1 a}{2\pi v_F}\right). \quad (8)$$

The scaling dimensions of the cosine terms in charge and spin channel are now given by

$$d_c = \frac{2}{\sqrt{1 + \frac{U_1}{\pi v_F}}}, \quad d_s = \frac{2}{\sqrt{1 - \frac{U_1}{\pi v_F}}}. \quad (9)$$

For a positive U_1, the scaling dimension $d_c < 2$. In this case, the Umklapp term is relevant. It opens a gap in the charge excitation spectrum. Qualitatively speaking, the smaller d_c (or larger U_1), the larger the charge gap Δ_c. Thus the forward scattering can enhance the charge gap. On the contrary, the

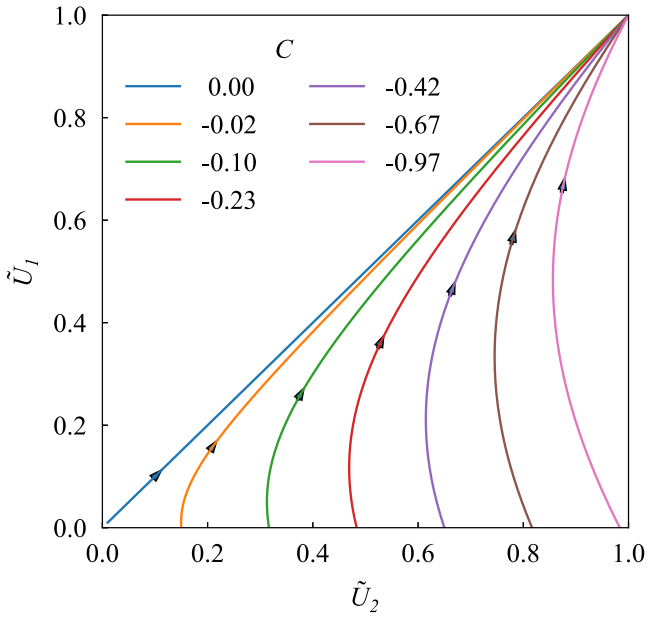

FIG. 3. RG flow of the coupling constants $\tilde{U}_1$ and $\tilde{U}_2$.

scaling dimension of the spin field $d_s > 2$ and the corresponding Umklapp scattering term is irrelevant. Consequently, the spin excitation remains gapless.

To quantitatively understand how the charge gap varies with the coupling constants, let us consider the scaling behavior of these parameters under the renormalization-group (RG) transformation. Larkin and Sak derived the RG equations of U_1 and U_2 to the third order of perturbation in the charge channel [39–42]. They obtained the following equations that govern the RG flow of U_1 and U_2 under the change of the scaling parameter l in the momentum cutoff $\alpha \to \alpha' = \alpha \exp(dl)$:

$$\frac{d\tilde{U}_1(l)}{dl} = 2\tilde{U}_2^2(l)[1 - \tilde{U}_1(l)], \tag{10}$$

$$\frac{d\tilde{U}_2(l)}{dl} = 2\tilde{U}_1(l)\tilde{U}_2(l) - \tilde{U}_1^2(l)\tilde{U}_2(l) - \tilde{U}_2^3(l), \tag{11}$$

where $\tilde{U}_i = U_i/(2\pi v_c)$ $(i = 1, 2)$.

From the above equations, it is straightforward to show that the variable

$$C = \frac{\tilde{U}_1^2(l) - \tilde{U}_2^2(l)}{1 - \tilde{U}_1(l)} \tag{12}$$

is scaling invariant and the RG equation governing $\tilde{U}_1$ is

$$\frac{d\tilde{U}_1(l)}{dl} = 2\big[\tilde{U}_1^2(l) + C\tilde{U}_1(l) - C\big][1 - \tilde{U}_1(l)]. \tag{13}$$

By solving this equation, we can find how the coupling constants $\tilde{U}_1$ and $\tilde{U}_2$ flow with l. The result, depicted in Fig. 3, shows that a strong-coupling fixing point exists at $\tilde{U}_1 = \tilde{U}_2 = 1$ in the large l limit: U_1 and U_2 always flow to this fixing point independent of their initial values.

In a gapped system, the correlation length is inversely proportional to the charge gap and upper bound by the charge gap. Consequently, l is also constrained by the charge gap $l < l_s = \ln[\beta v_c k_F/\Delta_c(U_1, U_2)]$, where l_s is the increment of the coupling constants along the trajectory from (U_1, U_2) to the final point (U_{1s}, U_{2s}), which are close to the point (1,1). $\beta v_c k_F$ is the characteristic energy scale that measures the effective charge gap at (U_{1s}, U_{2s}) and β is a coefficient that depends on (U_{1s}, U_{2s}). $k_F = \pi/(2a)$ is the Fermi vector. From Eq. (13), we have

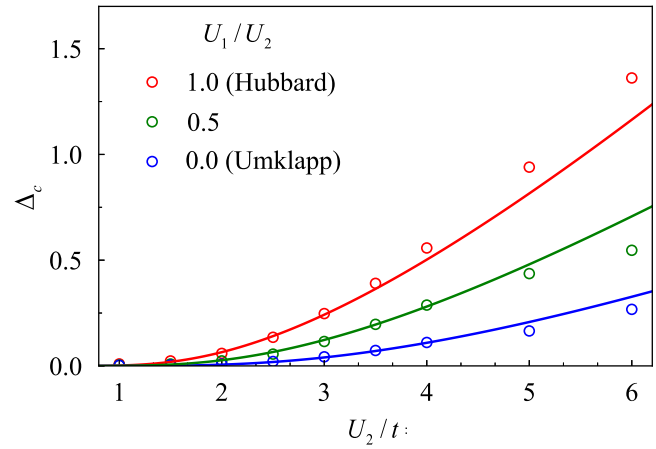

FIG. 4. Charge gap Δ_c as a function of U_2 for the generalized Hubbard model with three different values of U_1/U_2. The depicted curves represent results obtained from both bosonization (solid curves) and DMRG calculations (open circles). The DMRG results are obtained by extrapolating the calculations at finite L to the thermodynamic limit $L \to \infty$. The kDMRG calculations are performed for the generalized Hubbard models with $U_1/U_2 = 0$ and $U_1/U_2 = 0.5$ while retaining 8000 states. For the Hubbard model, real-space DMRG is employed, keeping 1000 states.

$$\int_0^{l_s} dl = \int_{\tilde{U}_1}^{\tilde{U}_{1s}} \frac{du}{2(u^2 + Cu - C)(1 - u)}. \tag{14}$$

Both integrals in the above equation are constrained along the trajectory with $C = C(\tilde{U}_{1s}, \tilde{U}_{2s})$. Solving Eq. (14), we obtain the expression of the charge gap

$$\Delta_c(U_1, U_2) = \beta v_c k_F e^{F(\tilde{U}_1) - F(\tilde{U}_{1s})}, \tag{15}$$

where

$$F(x) = -\frac{1}{2}\ln|1 - x| + \frac{1}{4}\ln(x^2 + Cx - C) + \begin{cases} \frac{C+2}{2C_1}\tanh^{-1}\frac{C+2x}{C_1}, & |C+2| > 2 \\ \frac{C+2}{2C_1}\tan^{-1}\frac{C+2x}{C_1}, & |C+2| < 2 \\ -\frac{1}{2x}, & |C+2| = 2 \end{cases} \tag{16}$$

and $C_1 = \sqrt{|C^2 + 4C|}$.

The Umklapp model with different U_2 has different scaling invariant parameters C. We need to determine the value of β at a given U_{1s} for each RG trajectory. However, the difference in the value of β between different trajectories at a given $\tilde{U}_{1s}$ is small in the limit $\tilde{U}_{1s} \to 1$ if $|C| \ll 1$. Hence we can use the value of β obtained by fitting the expression (15) on the trajectory $\tilde{U}_1 = \tilde{U}_2$ $(C = 0)$ with the DMRG results shown in Fig. 4 to determine the gap values of the Umklapp model. By taking $\tilde{U}_{1s} = 0.99$, we find that $\beta = 10.88 \pm 0.13$ (When fitting β, we only use data points with $U_2/t \leqslant 4.0$). Using this

parameter, we can estimate the gap values for the model with $\tilde{U}_1 \neq \tilde{U}_2$ and $|C| \ll 1$.

Figure 4 compares the results of Δ_c obtained by DMRG with those predicted by RG equations. For all the points shown in this figure, the corresponding values of $|C|$ are found to be less than 0.05, indicating that the condition $|C| \ll 1$ is satisfied. The agreement between the results obtained with these two approaches is excellent, except in the strong-coupling regime where the higher-order correction of perturbations to the RG equations should be considered. It confirms that the bosonization theory correctly catches up with the low-energy physics of the generalized Hubbard model, and the Mott insulating gap results from the Umklapp scattering of electrons around the Fermi level.

V. SUMMARY

In summary, we have analyzed the role of different scattering processes on the Mott insulating transition by invoking both kDMRG and bosonization methods. From the kDMRG calculation, we obtain for the first time the charge excitation gap as a function of the coupling constant for the one-dimensional Umklapp model. By comparing the results of the Umklapp model with that of the Hubbard model, we show that the Mott insulating gap is triggered by the Umklapp scattering, as expected, and that the forward scattering can strongly renormalize the gap value. In one dimension, the backward scattering weakly affects the Mott insulating gap. However, in two dimensions, the backward scattering may induce a long-range antiferromagnetic order and strongly interfere with the Umklapp scattering.

The interplay between different scattering processes enriches the physics of the Hubbard model. However, it also blurs the picture of the Mott metal-insulator transition, especially in two or higher dimensions, making it difficult to establish a quantum field theory description of the Mott insulator. In this work, we independently study the effect of each scattering process by screening some scattering processes in the one-dimensional Hubbard model. This strategy can be extended to two or higher dimensions. A project along this line is in progress. We hope it will allow us to capture the main physics governing the Mott metal-insulator transition and to find a general scheme for creating a quantum spin liquid by suppressing the antiferromagnetic order while keeping the Mott insulating gap open.

ACKNOWLEDGMENTS

This work is supported by the National Key Research and Development Project of China (Grants No. 2022YFA1403900 and No. 2017YFA0302901), the National Natural Science Foundation of China (Grants No. 12322403, No. 11888101, No. 11874095, and No. 11974396), the Youth Innovation Promotion Association CAS (Grants No. 2021004), and the Strategic Priority Research Program of Chinese Academy of Sciences (Grants No. XDB33010100, No. XDB0500202, and No. XDB33020300).

APPENDIX

1. Optimization of sites order

The interacting potential of the Umklapp model becomes highly nonlocal in real space, and it is hard to investigate this model using the real-space DMRG. In momentum space, on the other hand, this complexity can be significantly reduced. More specifically, one can dramatically lower the computational cost by minimizing the number of operators whose matrix elements need to be evaluated and stored in kDMRG from L^3 to $6L$ using the regrouping technique first introduced in Ref. [35] combined with the momentum conservation.

In momentum space, the lattice is a collection of all momentum-spin points (k, σ). Hence, a momentum-spin point now represents a lattice site. These momentum-spin points are ordered to form a one-dimensional lattice used for kDMRG calculations. In real space, the lattice sites have a natural order as the interactions are local. However, many ways exist to order the lattice sites in momentum space. Therefore, to optimize the kDMRG results, one needs first to optimize the order of these momentum-spin points. We do this in two steps:

First, starting from a trial order of the momentum-spin points guessed based on physical intuition, we perform the

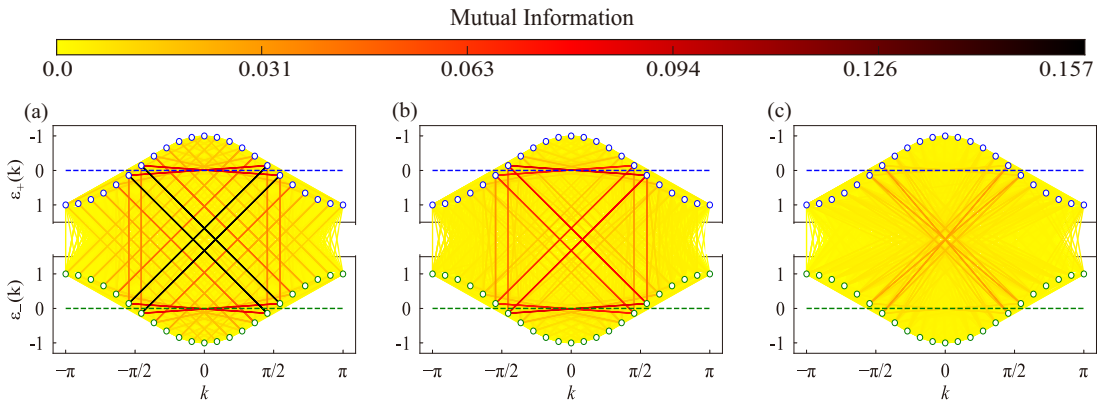

FIG. 5. Mutual information between two spin-momentum points in the ground states of the Hubbard, Umklapp ($U_2 = U$), and non-Umklapp ($U_1 = U$) models at half-filling. $U = 2.5t$ and $L = 22$. $\varepsilon_k = -2t \cos k$ is the energy dispersion of electrons in the absence of interactions. The plot looks symmetric because the vertical axis of the energy dispersion for the up-spin electrons is reversed. The dashed lines represent the Fermi levels.

standard kDMRG calculation to activate all the momentum-spin points. Then we sweep the lattice a couple of times. At each step, we swap two adjacent sites if the bipartite entanglement entropy between the left and right blocks separated by these two sites is lower than the case without swap.

Second, we calculate the mutual information between any two momentum-spin points, $M_{k\sigma,k'\sigma'}$, when the kDMRG sweep reaches the middle of the lattice. Then we rearrange all the lattice sites by minimizing the distance of two sites weighted by their mutual information:

$$M_{\text{dist}} = \sum_{k\sigma,k'\sigma'} |R(k\sigma, k'\sigma')|^2 M_{k\sigma,k'\sigma'}, \tag{A1}$$

where $R(k\sigma, k'\sigma')$ is the lattice distance between $(k\sigma)$ and $(k'\sigma')$. This minimization can further optimize the order of the momentum-spin points, preventing the ground state from being trapped in a local minimum.

2. Mutual information structure

Figure 5 shows the intensity plot of the mutual information between two momentum-spin points in the optimized ground state for the Hubbard, Umklapp, and non-Umklapp models with $U = 2.5$ at half-filling. The color scale of a line connecting two sites represents their mutual information. It is evident that electrons near the Fermi surface are most correlated in all three models, and the correlation between two electrons of different spins is stronger than that of the same spin.

For the Hubbard model, the checkerboard grid structure of the mutual information indicates that the two sites with a momentum separation π have a more apparent correlation than other sites. For the Umklapp model, the correlation structure is similar. However, looking at the mutual information structure more carefully, we find that the correlation decreases gradually when the two momentum-spin points move away from the Fermi surface. Moreover, a stronger correlation is observed between two electrons with the same momentum.

The subtle difference in the mutual information between the Hubbard and Umklapp models also appears in the momentum distribution function of electrons. Figure 6 shows the momentum distribution function n_k for the two models with two more electrons added to the half-fill system. For the Hubbard model, two added electrons tend to have opposite momentum, and the momentum of the ground state is zero. Therefore, n_k is mirror symmetric about the $k = 0$ point. However, for the Umklapp model, the two added electrons tend to have the same momentum, and n_k is nonsymmetric with respect to the central reflection point $k = 0$.

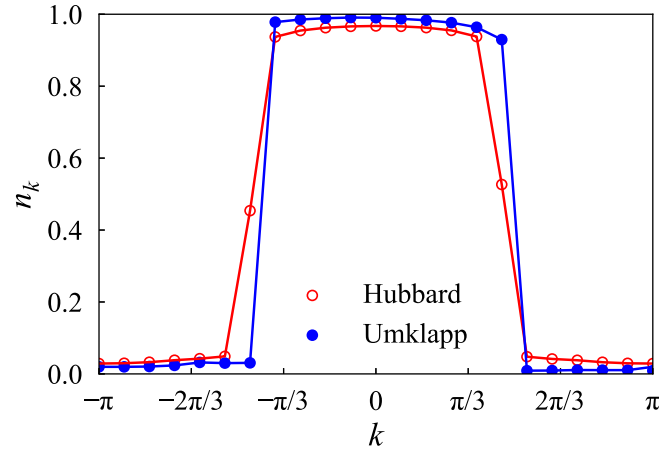

FIG. 6. Momentum distribution functions n_k of electrons in the ground state of the Hubbard and Umklapp ($U_2 = U$) models with $L + 2$ electrons. $D = 4000$ basis states are retained in the kDMRG calculation. $U = 2.5t$ and $L = 22$.

The correlation structure of the non-Umklapp model is distinctive from the former two models. In the non-Umklapp model, the backward scattering dominates. As a result, two electrons with opposite momentum show stronger correlations. The overall correlation of the non-Umklapp model is significantly weaker than the former two models. It suggests that the Umklapp scattering dominates the low-energy correlations of the Hubbard model.

[1] J. H. de Boer and E. J. W. Verwey, Proc. R. Soc. London A **49**, 59 (1937).
[2] N. Mott, *Metal-Insulator Transitions* (Taylor & Francis, London, 1990)
[3] F. Gebhard, *The Mott Metal-Insulator Transition*, Springer Tracts in Modern Physics, Vol. 137 (Springer-Verlag, Berlin, 1997).
[4] P. Phillips, Ann. Phys. (NY) **321**, 1634 (2006).
[5] M. B. J. Meinders, H. Eskes, and G. A. Sawatzky, Phys. Rev. B **48**, 3916 (1993).
[6] T. D. Stanescu, P. Phillips, and T.-P. Choy, Phys. Rev. B **75**, 104503 (2007).
[7] T. P. Choy, R. G. Leigh, and P. Phillips, Phys. Rev. B **77**, 104524 (2008).
[8] M. Imada, A. Fujimori, and Y. Tokura, Rev. Mod. Phys. **70**, 1039 (1998).
[9] R. S. Markiewicz, M. Z. Hasan, and A. Bansil, Phys. Rev. B **77**, 094518 (2008).
[10] T. D. Stanescu and P. Phillips, Phys. Rev. Lett. **91**, 049901(E) (2003).
[11] M. Hasan, E. Isaacs, Z. Shen, L. Miller, K. Tsutsui, T. Tohyama, and S. Maekawa, Science **288**, 1811 (2000).
[12] O. Parcollet and A. Georges, Phys. Rev. B **59**, 5341 (1999).
[13] M. Z. Hasan, P. A. Montano, E. D. Isaacs, Z.-X. Shen, H. Eisaki, S. K. Sinha, Z. Islam, N. Motoyama, and S. Uchida, Phys. Rev. Lett. **88**, 177403 (2002).
[14] P. A. Lee, N. Nagaosa, and X.-G. Wen, Rev. Mod. Phys. **78**, 17 (2006).
[15] J. Hubbard, Proc. R. Soc. London A **276**, 238 (1963).
[16] V. Bach, E. H. Lieb, and J. P. Solovej, J. Stat. Phys. **76**, 3 (1994).
[17] T. Giamarchi, Phys. Rev. B **44**, 2905 (1991).
[18] T. Giamarchi, Phys. B **230-232**, 975 (1997).
[19] H. J. Schulz, Phys. Rev. Lett. **64**, 2831 (1990).
[20] V. J. Emery, Phys. Rev. Lett. **65**, 1076 (1990).
[21] T. M. Rice, N. J. Robinson, and A. M. Tsvelik, Phys. Rev. B **96**, 220502(R) (2017).

[22] N. J. Robinson, P. D. Johnson, T. M. Rice, and A. M. Tsvelik, Rep. Prog. Phys. **82**, 126501 (2019).
[23] J. Klinovaja and D. Loss, Phys. Rev. Lett. **111**, 196401 (2013).
[24] C. Honerkamp, M. Salmhofer, N. Furukawa, and T. M. Rice, Phys. Rev. B **63**, 035109 (2001).
[25] W. Wu, M. Ferrero, A. Georges, and E. Kozik, Phys. Rev. B **96**, 041105(R) (2017).
[26] K.-Y. Yang, T. M. Rice, and F.-C. Zhang, Phys. Rev. B **73**, 174501 (2006).
[27] T. M. Rice, K.-Y. Yang, and F. C. Zhang, Rep. Prog. Phys. **75**, 016502 (2012).
[28] L. Balents and M. P. A. Fisher, Phys. Rev. B **53**, 12133 (1996).
[29] C. J. Halboth and W. Metzner, Phys. Rev. B **61**, 7364 (2000).
[30] E. H. Lieb and F. Y. Wu, Phys. Rev. Lett. **20**, 1445 (1968).
[31] E. H. Lieb and F. Y. Wu, Phys. Rev. Lett. **21**, 192 (1968).
[32] S. Daul and R. M. Noack, Z. Phys. B **103**, 293 (1996).
[33] R. Arita, K. Kuroki, H. Aoki, and M. Fabrizio, Phys. Rev. B **57**, 10324 (1998).
[34] A. W. Sandvik, D. J. Scalapino, and C. Singh, Phys. Rev. B **48**, 2112 (1993).
[35] T. Xiang, Phys. Rev. B **53**, R10445 (1996).
[36] V. Emery, *Highly Conducting One-Dimensional Solids* (Plenum, New York, 1979).
[37] V. J. Emery, A. Luther, and I. Peschel, Phys. Rev. B **13**, 1272 (1976).
[38] G. Ehlers, J. Sólyom, O. Legeza, and R. M. Noack, Phys. Rev. B **92**, 235116 (2015).
[39] A. I. Larkin and J. Sak, Phys. Rev. Lett. **39**, 1025 (1977).
[40] G.-H. Ding, F. Ye, and B.-W. Xu, Commun. Theor. Phys. **39**, 105 (2003).
[41] K. Penc and F. Mila, Phys. Rev. B **50**, 11429 (1994).
[42] M. Mariño and T. Reis, Phys. Rev. B **106**, 125142 (2022).